

A METHOD FOR SNOW-COVER MAPPING OF FORESTS BY OPTICAL REMOTE SENSING

Dagrun Vikhamar¹ and Rune Solberg²

*¹Department of Physical Geography, University of Oslo, P.O. Box 1042 Blindern,
N-0316 Oslo, Norway,*

Phone: +47-2285-5804, Fax: +47-2285-7230, E-mail: dagrun.vikhamar@geografi.uio.no

²Norwegian Computing Center, Oslo, Norway

ABSTRACT

A snow-covered forest mapping method for optical remote sensing is proposed. The method is based on linear sub-pixel reflectance modelling of the surface components snow, individual tree species and bare ground. Experiments are performed using a 100% snow-covered Landsat TM scene and aerial photos covering spruce, pine and birch forest in the Jotunheimen mountain area of South Norway. The reflectance modelling shows best results for pine forest and mixed pine and birch forest, while the modelled reflectance for birch forest and spruce forest is underestimated. The results are improved when tree shadows on the snow surface and reduced diffuse illumination due to tree crowns masking parts of the sky hemisphere are included in the reflectance model.

INTRODUCTION

Seasonal snow may cover up to 50 million km² (34%) of the Earth's land surface (1). Most of the seasonal snow is located in the Northern Hemisphere. Boreal forest covers 12 million km² (8%) of the land surface, and most of the boreal forest is seasonally snow covered. Seasonally snow-covered forest is also present in high mountain regions of temperate latitudes.

Monitoring the snow-cover extent is important both for climatological studies and for hydrological applications. Due to the high snow albedo compared to other natural surfaces, variations in the global snow-cover distribution affect the global energy balance. Hydrological applications include support to hydropower production planning and river flood predictions.

Several classification methods have been developed for or adapted to optical snow-cover mapping, e.g. the SNOMAP-algorithm (2), linear spectral unmixing (3), and an empirical linear sub-pixel classification method (4). The classification methods give reasonable results for unforested areas, see e.g. (2). However, forested areas constitute a problem due to the contribution of radiance from the trees, in addition to reducing the radiance from the snow below the trees. Classification methods generally underestimate the snow cover in forest, see e.g. (5). The SNOMAP-algorithm has been extended by including the Normalized Difference Vegetation Index to map snow-covered forest (6), and verification of the algorithm is investigated by (7).

The objective of this work is to study the possibilities for determining the snow coverage at sub-pixel level in forest by optical remote sensing. A snow-cover mapping method, based on linear sub-pixel reflectance modelling, is proposed. Experiments focus on physical reflectance modelling in order to understand the various factors that influence on the satellite-measured reflectance from a snow-covered forest. By examining the temporal influence of these factors on the pixel reflectance, a simplified operational model may later be derived. The experiments deal with 100% snow-covered spruce, pine and birch forest, and mixed pine and birch forest, while situations of less than 100% snow coverage will be investigated in a later work. Three successive experiments are presented and discussed: 1) The snow surface is modelled entirely illuminated; 2) The tree shadows on the snow surface are included in the reflectance model; and 3) The reduced diffuse illumination

reaching the snow surface due to surrounding trees that reduce the visible sky hemisphere is modelled and included in the reflectance model.

THE SNOW-COVERED FOREST MAPPING METHOD

During the snowmelt season, the satellite measured radiance from a snow-covered forest is influenced by a number of surface components, illumination- and atmospheric effects. The main surface components of a snow-covered forest are trees, snow and bare ground. The spectral radiance of each surface cover is affected by the temporal natural variability of the surface cover. Based on the influence of the temporal natural variability on the radiance, a variability ranking of the surface components is made. Snow is temporally the most unstable surface component (diurnally and seasonally). The snow metamorphosis, which is a continuous process, changes the physical properties of the snow. The snow albedo may vary between 35% and 90% (1). Bare ground consists of vegetation, vegetation litter, rocks and soils. Bare ground is ranked as the second most influencing surface component, provided that the vegetation is non-green and the temporal moisture conditions are stable. Dry, snow free conifer and non-green deciduous trees are the least changing surface components, giving the most stable influence on the radiance. Added to these surface components are the direct and diffuse illumination effects, which are due to solar elevation angle, trees and topography. Shadows on the snow/ground surface and shadows in the tree crowns are direct illumination effects, and occur due to single trees. Surrounding trees may increase these shadowed areas (mutual shadowing). Trees also reduce the sky hemisphere visible from the snow/ground surface, and consequently reduce the diffuse illumination reaching the snow/ground surface. Additionally, these direct and diffuse illumination effects are affected by the topography. Among these illumination effects direct illumination effects due to single trees are considered as first order effects, while second order effects are mutual shadowing and diffuse illumination.

Based on the ranking of the surface components and first order illumination effects, a linear sub-pixel reflectance model, which is an area-weighted sum of these components, is proposed for the modelling:

$$R = A_P R_P + A_S R_S + A_B R_B + A_{SW} R_{SW} + A_{SWP} R_{SWP} + A_{SWS} R_{SWS} + A_{SWB} R_{SWB} + A_{BG} R_{BG},$$

where R is the pixel reflectance, A_P , A_S , A_B are the area proportions of a pixel covered by pine, spruce and birch tree crowns, respectively. A_{SW} and A_{BG} represent the area proportions covered by illuminated snow and bare ground, respectively. R_P , R_S , R_B are the tree-crown reflectances of pine, spruce and birch, respectively. R_{SW} is the illuminated snow reflectance, while R_{BG} is the bare ground reflectance. Shadows within the tree crowns are included in the model using tree-crown reflectances representing the combined illuminated and shadowed tree crowns. A shadowed snow component for pine (A_{SWP} , R_{SWP}), spruce (A_{SWS} , R_{SWS}) and birch (A_{SWB} , R_{SWB}) models the tree shadows on the snow. Spruce and pine tree crowns are assumed opaque, while leafless birch tree crowns are assumed transparent. Therefore, birch tree crown reflectance (R_B) is modelled separately by linear mixing of illuminated snow (A'_{SW} , R_{SW}) and estimated effective branch area proportion (A'_B , R'_B): $R_B = A'_{SW} R_{SW} + A'_B R'_B$ (Figure 1). The effective branch area proportion is the proportion of birch branches within a tree crown, projected vertically on the snow surface. The effective branch area proportion is estimated using the tree height (h) as input parameter to the regression function $A'_B = ah + b$. Similarly, the reflectance of the shadowed snow component of birch (R_{SWB}) is modelled separately using a linear mixing reflectance model of illuminated snow (A''_{SW} , R_{SW}) and estimated effective shadow area proportion (A'_{SWB} , R'_{SWB}): $R_{SWB} = A''_{SW} R_{SW} + A'_{SWB} R'_{SWB}$. The effective shadow area proportion is also estimated from the tree height (h): $A'_{SWB} = ch + d$.

Some assumptions are made for the snow-covered forest mapping method. When the forest is observed from nadir, parts of the snow/ground surface must be visible. The ground area covered by a pixel is assumed to be greater than the size of individual trees. The tree-crown reflectance is

assumed constant for a given solar elevation angle and the area covered by tree crowns is constant during a snowmelt season. The tree crowns are assumed dry and snow free.

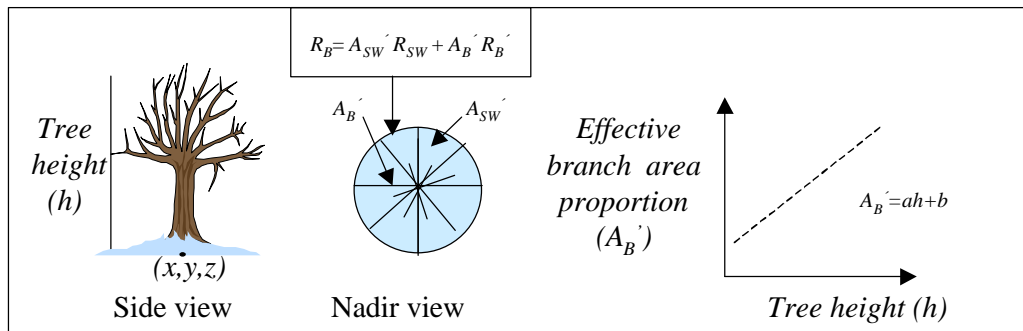


Figure 1: Birch tree crown reflectance (R_B) is modelled by linear mixing of illuminated snow and effective branch area proportions of vertically projected tree crowns. The effective branch area is estimated based on the tree height. An empirical regression function has been developed from measurements of trees of various tree heights.

DATA SET

A study area with maximum 10° terrain slope in the Jotunheimen mountain area of South Norway (9°E , 61°N , approximately 900 m.a.s.l.) covering sparse forest of spruce (*Picea abies*), pine (*Pinus sylvestris*) and mountain birch (*Betula pubescens* ssp. *czerepanovii*) was selected for experiments (Figure 2). The data set consisted of a Landsat TM scene, infrared aerial photos and fieldspectrometer measurements.

Three strips of infrared aerial photos (1:15,000, 70 km^2) from August 1998 served as reference data for a 100% snow-covered Landsat TM scene from 21 April 1998 (37.4° solar elevation angle). Three sub-areas (19 km^2) were selected for detailed measurements of individual trees using a high-precision analogue photogrammetric instrument (Stereosimplex G6). A forest model representation was generated by measuring the tree species, the tree height, the tree-crown diameter and the position of each tree. In total 14,511 birch trees, 13,611 pine trees and 1652 spruce trees were measured. These data served to determine the tree crown area proportions of the reflectance model, in addition to calculating the shadowed areas of the snow surface.

Sub-areas of the Landsat TM image were geometrically corrected using coordinates from the aerial photos. The satellite image pixel values were calibrated to ground reflectance using spectral signature of tap water (8) and in-situ field measured snow spectral signatures. The reflectance calibration eliminated TM5 and TM7 due to low water and snow reflectance. TM1 was excluded due to pixel saturation from high snow reflectance.

A portable FieldSpec spectrometer (350-2500 nm, 2151 channels) and a calibrated white spectralon reference target were used to measure in-situ spectral signatures of illuminated snow, shadowed snow from individual tree species, tree crown reflectance of spruce and pine, and branches of birch trees. Integrated Landsat TM reflectance values were calculated from the spectral signatures.

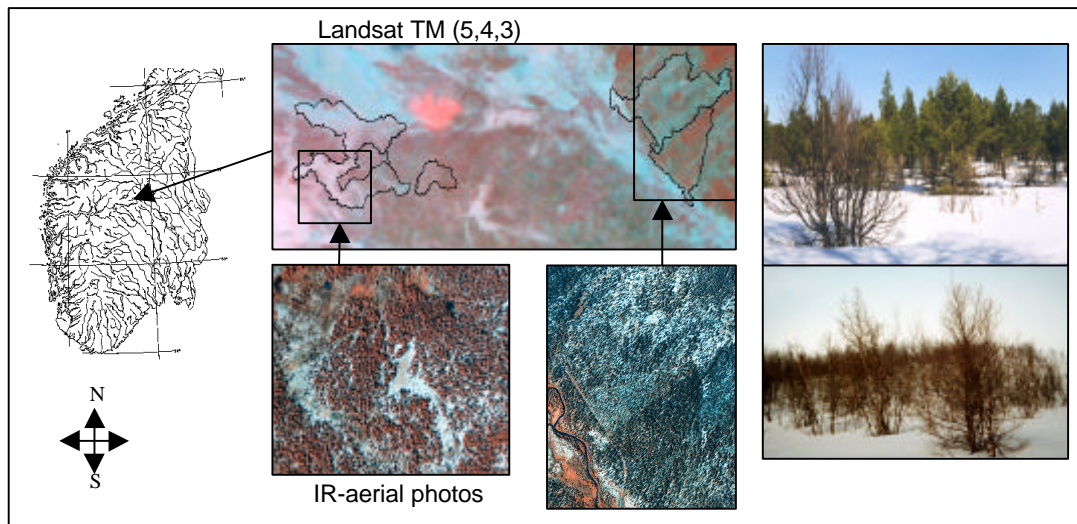


Figure 2: The study area in the Jotunheimen mountain area of South Norway. The figure shows a sub-image of the Landsat TM scene with two of the sub-areas where individual trees were measured. The aerial photo to the left shows mainly birch forest, while the aerial photo to the right shows mainly pine forest. White areas in the TM-scene are unforested snow-covered areas. The two photographs to the right illustrate the pine forest and the birch forest.

EXPERIMENTS

The experiments in the work described here focus on situations with 100% snow coverage, thus the bare ground component is eliminated. This is to reduce the number of effects in a first stage of investigation. The following data sets were analysed: A. Snow and pine forest (596 pixels); B. Snow and spruce forest (182 pixels); C. Snow and birch forest (506 pixels); and D. Snow and mixed pine and birch forest (810 pixels). The number of pixels covering other combinations of tree species was too low for statistical analysis. Statistics for the area proportions of the tree crowns and the tree crown shadows, used in the reflectance modelling of each data set, are shown in [Table 1](#). Three experiments with the data sets A-D are carried out, of which the subsequent experiments are extensions to the previous experiments by integrating more components into the reflectance model. The motivation for this approach is to start with the simplest situation, and further refine the reflectance modelling. The three experiments consist of: 1) Modelling totally illuminated snow surface; 2) Include tree shadows on the snow (first order illumination effect); and 3) Model the reduced diffuse illumination reaching the snow surface (second order illumination effect). The results from the three experiments were evaluated against the measured Landsat TM reflectance ([Figure 5](#), [Table 3](#)). Measured TM2-4 reflectance were highly correlated ($R^2=0.97-0.99$), therefore only TM3 is presented.

1. Reflectance modelling with totally illuminated snow surface

In the first experiment the snow was modelled totally illuminated for data sets A-D. The integrated TM2-4 reflectance values of snow, spruce tree crowns, pine tree crowns and branches of birch trees, which were applied for the reflectance modelling, are shown in [Table 2](#). The birch branch reflectance (R_B') was calculated by a solar elevation adjusted mixture of illuminated and shadowed branch spectral signatures. The proportion of illuminated branches of a birch tree crown, when observed from nadir, was estimated by modelling the birch trees to consist of horizontal cylinder shaped branches. 0° and 90° solar elevation angle would give 25% and 100% illuminated branches, respectively, when viewed from nadir. Assuming a linear function using these values, 37.4° solar elevation angle gives 56.2% illuminated branches and 43.8% shadowed branches. The birch branch reflectance was calculated using these values. The tree crown area proportions of pine, spruce and

birch (A_P , A_S , A_B) were determined using the forest model representation. The area of vertically projected tree crowns located inside the TM pixels was calculated by drawing circles defined by the measured tree crown diameters and the tree positions. The applied regression function for estimating the effective branch area proportion of birch tree crowns is described below.

2. Reflectance modelling accounting for tree shadows on the snow surface

In the second experiment, shadowed snow was included by integrating a shadowed snow component for each tree species. The shadowed area proportions (A_{SWP} , A_{SWS} , A_{SWB}) were determined by calculating the shadowed ground area of each tree based on its tree height, tree crown diameter, the solar elevation angle, the solar azimuth angle and modelling the trees as cylinders with a spherical top (Figure 3). The method for calculating the individual tree shadows was verified by estimating shadows for the time of aerial photo acquisition, and visually compare the real shadows and the modelled shadows in 3D using a digital photogrammetric workstation. TM2-4 reflectance values were derived from field measured spectral signatures of shadowed snow from individual pine, spruce and birch trees (Table 2). Initially, the regression functions for determining the effective birch branch area proportion and the effective shadow area proportion were: $A_B' = 4.7 h + 20.5$ and $A_{SWB}' = 3.9 h + 16.8$. These functions were determined empirically using field measured spectral signatures of entire tree crowns, single branches and shadows of birch trees of variable heights. Birch trees in lower areas (450 m.a.s.l.) near Oslo, Norway, were measured. Since the environmental conditions in mountainous regions are severe compared to the lower areas, mountain birch was believed to grow more slowly and develop more branches for the same tree height as lowland birch. Therefore, the empirical regression functions were refined by additional measurements of mountain birch near the study area. The resulting regression functions, applied in the experiments, were: $A_B' = 7.6 h + 13.5$ and $A_{SWB}' = 6.8 h + 9.9$. The average tree height (h) for single TM pixels were input to the regression functions.

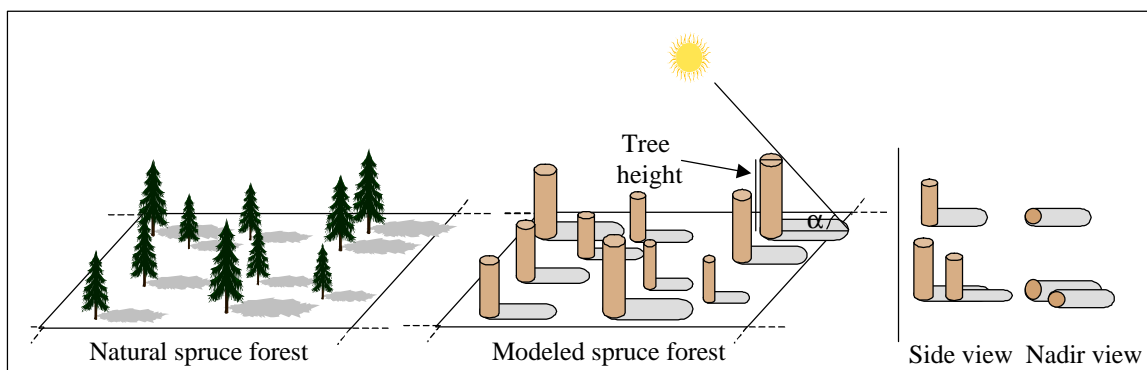


Figure 3: The shadow on the snow surface of each tree is calculated using the tree height, the tree crown diameter, the solar elevation and azimuth angle, and a cylinder model of the tree. The shadowed area proportion was calculated as the fraction of shadowed areas within a pixel compared to the pixel area.

3. Reflectance modelling accounting for reduced diffuse illumination

The reflectance model does not account for second order illumination effects (mutual shadowing and reduced diffuse illumination reaching the snow surface due to trees masking parts of the sky hemisphere). As a first approach it was focused on modelling the diffuse illumination, while the effects of mutual shadowing will be investigated in later work. A method for modelling the diffuse illumination is proposed, and tested for pure pine, spruce and birch forest.

The diffuse illumination reaching a point on the snow surface is directly related to the proportion of the sky hemisphere visible from the point (9). Trees surrounding a horizontal snow surface reduce the hemisphere visible from the snow surface (Figure 4), and consequently reduce the amount of diffuse illumination. A method that accounts for the reduced diffuse illumination may include two steps: 1) Estimate the visible part (J) of the hemispherical area from the snow surface for a pixel. 2)

Based on a 100% visible hemisphere, reduce the diffuse illumination of the snow reflectance components (R_{SW} , R_{SWS} , R_{SWP} , R_{SWB}) to the pixel's estimated visible part of the hemisphere. According to the assumptions for the snow-covered forest reflectance model, spruce and pine are assumed opaque while birch is assumed transparent. Different methods are, therefore, developed to estimate the mean incoming diffuse illumination to the pixel (Figure 4).

Pine and spruce are modelled as cylinders, and positioned in a regular pattern with equal distance between the trees, defined by the pixel's mean tree distance. The visible part of the hemispherical area is estimated for each pixel by: $I = aI_1 + bI_2 + cI_3$, where I_1 and I_2 are the estimated visible fractions of the hemisphere between the observation point and the closest trees and the distant trees, respectively. I_3 represents open areas in the azimuth directions between the closest and the distant trees where the visible fraction of the hemisphere is 100%. I_1 and I_2 are calculated using the mean tree height and distance, r_1 and r_2 , from the observation point. a , b and c are weights representing the azimuth directions for I_1 , I_2 and I_3 , respectively.

Due to the transparency of birch tree crowns, another method was applied for birch forest. The volume of the branches of the birch trees inside a pixel is estimated using the empirical regression function for the effective branch area proportion ($A_B' = 7.6 h + 13.5$). The branches are evenly distributed within a canopy layer, which is the volume

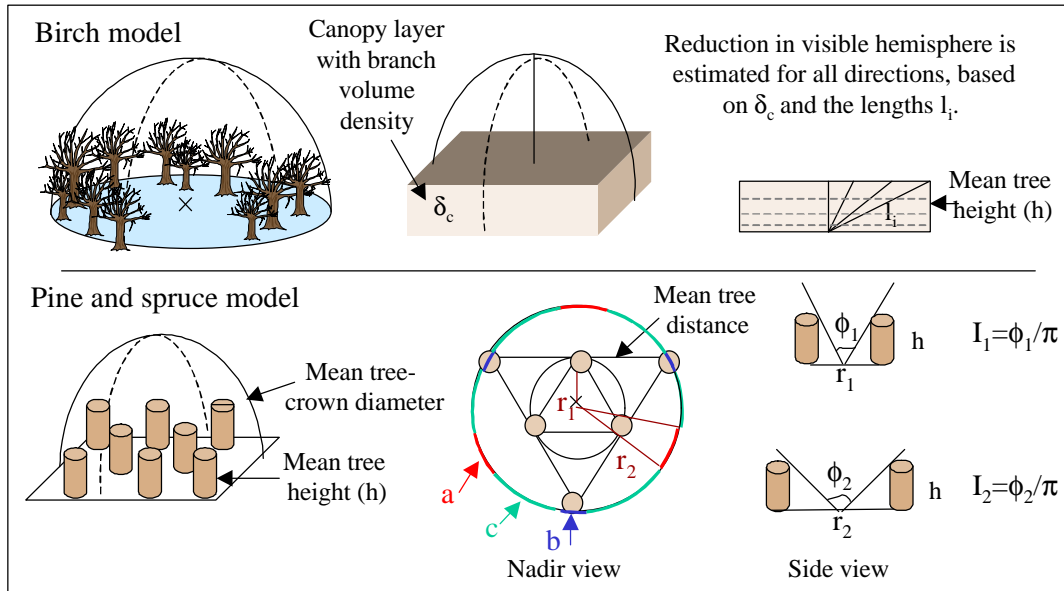


Figure 4: Modelling of diffuse illumination for birch, pine and spruce forest. Birch forest is modelled by an even distribution of branches within a canopy layer defined by the pixel area and the pixel's mean tree height. Pine and spruce forest are modelled by positioning the trees in a regular pattern with equal distance between the trees, defined by the pixel's mean tree distance.

defined by the pixel area and the pixel's mean tree height. Based on the estimated branch volume within the canopy layer, a pixel's branch volume density (d_c) is estimated. Reduction of the visible part of the hemisphere is estimated for all directions based on the branch volume density and the length through the canopy layer the light passes from an observation point. The spherical area of the hemisphere may be calculated by an integral (9), but a simplified method was applied. The visible part of the hemisphere (I) was estimated by subdividing the hemisphere into many layers (i) and summing up the layers' estimated visible fractions of the hemisphere (I_i) and the layers' area proportions (P_i) of the total hemispherical area: $I = \sum_i P_i I_i$.

Based on a 100% visible hemisphere, the diffuse illumination of the snow reflectance components (R_{SW} , R_{SWP} , R_{SWS} , R_{SWB}) were reduced to the estimated visible part of the hemisphere. Integrated

Landsat TM reflectance values for diffuse illumination for 100% visible hemisphere was derived from field spectrometer measurements (48° solar elevation angle): TM1: 22.4%, TM2: 13.9%, TM3: 8.7%, TM4: 4.8%, TM5: 1.3%, TM7: 0.9%. These reflectance values were determined by measuring diffuse illumination reflected from the spectralon reference target for 50% visible hemisphere, using a vertically placed plate covered by a 100% absorbing black material.

4. Sensitivity test of the geometric co-registration

To evaluate the correctness of the geometric co-registration of the aerial photos and the Landsat TM sub-images a sub-pixel correction was performed. By doing this, the sensitivity of the modelling results was also tested. The geometric co-registration was evaluated by moving the x- and y coordinates of the aerial photos every 1 m from -20 m to +20 m related to the starting position $x,y=0,0$ (the original geometric co-registration). Regression functions for measured and modelled reflectance (experiment 2) were calculated for each position. The criterion for finding the optimised geometric co-registration was the position that gave the highest R^2 value. In total 1681 positions were evaluated for each of the Landsat TM sub-images. Results for the data sets A-D are presented in [Table 4](#).

RESULTS

A comparison of the measured and the modelled Landsat TM reflectance was performed by linear regression. An ideal model would give the slope 1, the intercept 0 and the R^2 value 1. A ranking of the results for experiment 1, based on the regression equations, shows this order for the data sets (see [Table 3](#)): 1) The snow and pine forest; 2) The snow and birch forest, and the snow and mixed pine and birch forest; and 3) The snow and spruce forest. Experiment 2 gives approximately the same ranking, except that the snow and mixed pine and birch forest model is better than the snow and birch forest model. Experiment 3 gives the ranking: 1) The snow and pine forest; 2) The snow and birch forest; and 3) The snow and spruce forest.

This shows that best results were obtained for the snow and pine forest model and the mixed pine and birch forest model. Both the snow and birch forest model and the snow and spruce forest model underestimate the reflectance. An important result is that all the regression equations are significantly improved when shadows are included in the reflectance model (experiment 2), while including diffuse illumination only gives small changes (experiment 3).

The results from the sub-pixel correction of the geometric co-registration showed that displacements of a few meters of the x,y coordinates gave the best R^2 values ([Table 4](#)). However, the regression equations were approximately the same as for the original geometric co-registration (experiment 2 in [Table 3](#)). With increasing distance from the original geometric co-registration ($x,y>10$ m) the regression equations and the R^2 values deteriorated considerably.

*Table 1: Area proportions (%) of a pixel for the data sets: A. Snow and pine forest; B. Snow and spruce forest; C. Snow and birch forest; and D. Snow and mixed pine and birch forest. **m** = mean value, **s** = standard deviation.*

Data set		Area proportions					
		A_P	A_S	A_B	A_{SWP}	A_{SWS}	A_{SWB}
A	m	8.1	-	-	32.5	-	0.2
	s	5.5	-	-	14.0	-	0.6
B	m	-	3.7	-	-	17.7	0.0
	s	-	2.7	-	-	12.6	0.2
C	m	-	-	6.9	0.2	-	17.5
	s	-	-	6.2	0.8	-	13.0
D	m	6.6	-	3.9	24.3	-	10.1
	s	5.0	-	4.1	14.9	-	10.1

Table 2: *TM2-4 reflectance (%) for the area components of the reflectance model. Values are derived from spectral signatures using FieldSpec spectrometer.*

Area component	TM2	TM3	TM4
Illuminated snow (R_{SW})	92	89	77
Pine tree crowns (R_P)	12	7	47
Spruce tree crowns (R_S)	10	6	48
Birch branches (R_B')	10	11	23
Pine, shadowed snow (R_{SWP})	14	9	8
Spruce, shadowed snow (R_{SWS})	20	17	16
Birch, shadowed snow (R_{SWB}')	26	21	16

Table 3: *Estimated regression parameters from measured and modelled Landsat TM3 reflectance.*

Data set	Experiment	Slope	Intercept	R ²
A	1	0.33	66.14	0.50
	2	1.17	-1.12	0.56
	3	1.20	-4.34	0.56
B	1	0.09	79.58	0.38
	2	0.51	35.59	0.54
	3	0.52	33.04	0.54
C	1	0.24	68.89	0.48
	2	0.67	31.87	0.62
	3	0.72	27.29	0.61
D	1	0.23	70.36	0.43
	2	0.93	11.86	0.55

Table 4: *Estimated regression parameters from measured and modelled Landsat TM3 reflectance for the optimised geometric co-registration. x,y values (m) are displacement from the original x,y position = 0,0.*

Data set	x, y	Slope	Intercept	R ²
A	+3,-3	1.16	-0.30	0.60
B	-8,-1	0.55	32.74	0.64
C	-6,+6	0.68	31.70	0.66
D	+3,+5	0.95	10.58	0.60

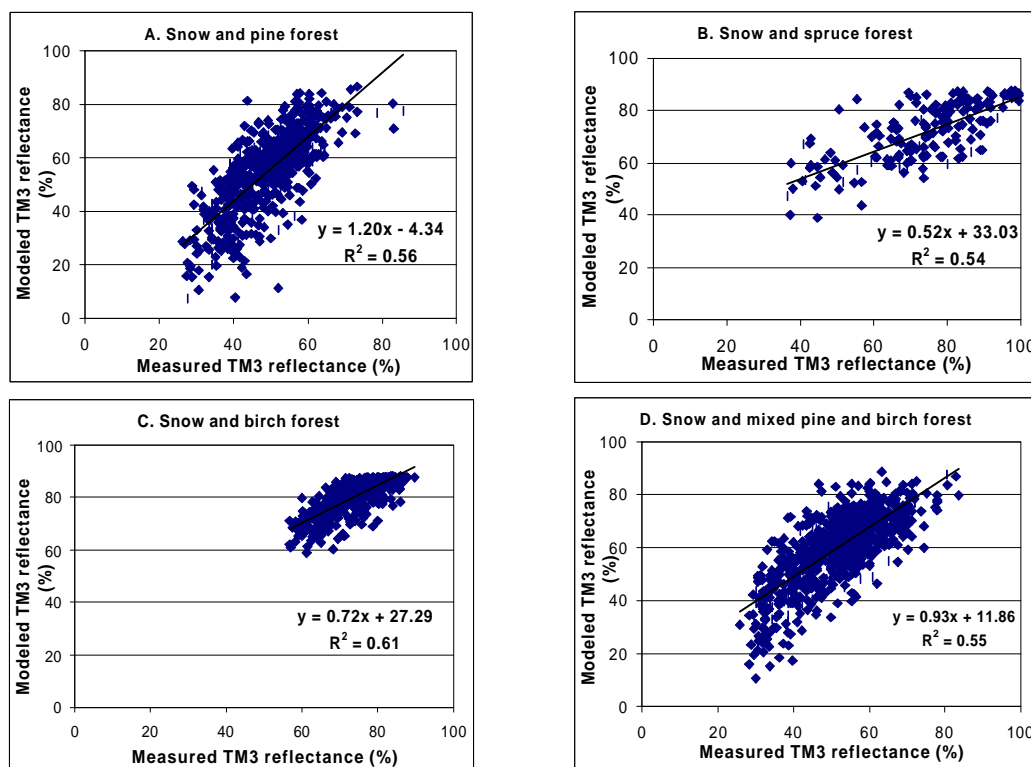


Figure 5: Measured and modelled Landsat TM3 reflectance for the data sets A-D. Modelled reflectance includes tree shadows and diffuse illumination for data sets A-C (experiment 3). Data set D includes tree shadows (experiment 2).

DISCUSSION AND CONCLUSIONS

One of the aims of physical reflectance modelling is to investigate the influence of the various surface components and illumination effects on the measured pixel reflectance, and be able to select the important effects that could be included in a generalised operational model for snow-cover mapping of forested areas. The results from the experiments in this work clearly demonstrated that the main surface components snow and individual tree species, in addition to first order illumination effects (shadows in the tree crowns and on the snow surface due to single trees) are the most important components. For modest solar elevation angles in sparse forest, shadows on the snow surface may cover great areas compared to the tree crowns.

The modelling results were much better for the pine forest than for the spruce forest, even though pine and spruce have similar morphology. Both the data set and the range of tree crown area proportions (A_P and A_S) were larger for the pine forest than for the spruce forest. Unfortunately, cumulus clouds in the Landsat TM scene covered areas of dense spruce forest. The scatter plot of the mixed pine and birch forest has an elliptic shape, which probably is due to underestimation of birch forest reflectance and overestimation of pine forest reflectance.

Modelling of diffuse illumination (second order illumination effect) gave small improvements of the results. The influence of this effect is wavelength dependent, and decreases with increasing wavelength. The results may indicate that diffuse illumination is an effect of less importance. The methods for modelling the diffuse illumination simplify the nature, and the correctness is not quantified. Both methods are based on the same principle, which consists of an even distribution of trees located inside a pixel (pine trees, spruce trees and birch branches). In natural distributions, clustering is very common. Clustering of trees increases the illumination effects. Therefore, by positioning the trees in a regular pattern, the reduction of the diffuse illumination may be underestimated. The shadowed snow reflectance values in [Table 2](#) are higher than the measured

reflectance values for diffuse illumination for 100% visible hemisphere. Possible reasons for the discrepancies are different solar elevation angles and different atmospheric conditions during the field measurements.

A general problem for all the modelling results is the large degree of scattering, which may be due to second order illumination effects and topographic influence that are not accounted for in the reflectance model. Other error sources may be attributed to the assumptions made for the snow-covered forest mapping method. The linear sub-pixel reflectance model assumes that radiative processes of the surface components are independent of their area proportions within the pixel. Green leaves may produce non-linear scattering in near infrared wavelengths. However, the birch trees were leafless and for conifer trees the effect is small. The assumption of modelling spruce and pine tree crowns opaque is a simplification, because pine tree crowns generally are more open than spruce tree crowns. If the snow below the tree crowns contributes to the satellite-measured reflectance, then it probably concerns small trees, and more frequently pine than spruce.

The criterion used for evaluating other positions of the geometric co-registration was the R^2 value. This means that the geometric co-registration was optimised with respect to the data set. This is not an objective evaluation method of the co-registration in itself. The optimised positions were found to be located within a few metres from the original geometric co-registration for all the data sets, and still the regression equations remained approximately unchanged. The deterioration of the regression equations for positions with increased distance (>10 m) from the original geometric co-registration indicate that the original co-registration was correct. Generally, small displacements of a few metres, therefore, influenced the modelling results very little.

The results from this work show that sub-pixel reflectance modelling of snow-covered sparse forest is possible. In order to explain the scattering, further research will be performed on modelling illumination effects and topographic influence that are not already accounted for in the reflectance model. Also, situations of partly snow-covered forest will be studied. Based on the physical reflectance modelling a general operational model will be derived. The concept for an operational model for snow-cover mapping of forests will be based on existing forest information (maps and statistics) or classification of high-resolution satellite images to determine the area proportions of the individual tree species. A spectral library of snow, bare ground and tree crown reflectances for various solar elevation angles will be established and used to retrieve the reflectance values for the sub-pixel reflectance model.

ACKNOWLEDGMENTS

This work was supported by SNOWTOOLS, an environment and climate project, funded by the Commission of the European Communities, contract no. ENV4-CT96-0304, and the Department of Physical Geography, University of Oslo, Norway.

REFERENCES

1. Hartmann, D.L. 1994. Global Physical Climatology. (Academic Press)
2. Hall, D.K., Riggs, G.A. and Salomonsen, V.V. 1995. Development of methods for mapping global snow cover using Moderate Resolution Imaging Spectroradiometer Data. Remote Sensing of Environment. 54:127-140.
3. Nolin, A.W., Dozier J. and Mertes, L.A.K. 1993. Mapping alpine snow using a spectral mixture modeling technique. Annals of Glaciology. 17:121-124.
4. Solberg, R. and Andersen, T. 1994. An automatic system for operational snow-cover monitoring in the Norwegian mountain regions. Proceedings of IGARSS'94 Symposium:2084-2086. Pasadena, California, USA.

5. Solberg, R. et al. 1997. Snow algorithms and products - Review and recommendations for research and development. Project SNOWTOOLS WP 410, NR Report No. 924. (Norwegian Computing Center, Oslo)
6. Hall, D.K. et al. 1998. Assessment of snow-cover mapping accuracy in a variety of vegetation-cover densities in Central Alaska. Remote Sensing of Environment. 66:129-137.
7. Klein, A.G., Hall, D.K. and Riggs, G.A. 1998. Improving snow-cover mapping in forests through the use of a canopy reflectance model. Hydrological Processes. 12:1723-1744.
8. The Johns Hopkins University Spectral Library. <http://speclib.jpl.nasa.gov/>
9. Proy, C., Tanré, D. and Deschamps, P.Y. 1989. Evaluation of topographic effects in remotely sensed data. Remote Sensing of Environment. 30:21-32.